Contrasting the flavors of El Niño-Southern Oscillation using sea surface salinity observations

Awnesh Singh, Thierry Delcroix, Sophie Cravatte

Contrasting the flavors of El Niño-Southern Oscillation using sea surface salinity observations

Awnesh Singh,[1] Thierry Delcroix,[1] and Sophie Cravatte[1]

Received 3 December 2010; revised 25 February 2011; accepted 9 March 2011; published 23 June 2011.

[1] The recent detection of a central Pacific type of El Niño has added a new dimension to the El Niño-Southern Oscillation climatic puzzle. Sea surface salinity (SSS) observations collected during 1977–2008 in the tropical Pacific are used to contrast the three eastern Pacific (EP) (1982–1983, 1991–1992, 1997–1998) and seven central Pacific (CP) (1977–1978, 1986–1988, 1990–1991, 1992–1995, 2002–2003, 2004–2005, 2006–2007) types of El Niño events, as well as the six EP (1985–1986, 1988–1989, 1995–1996, 1999–2001, 2005–2006, 2007–2008) and two CP (1983–1984, 1998–1999) types of La Niña events. The EP El Niño events result in large (~30° longitude) eastward displacements of the eastern edge of the low-salinity warm pool waters in the equatorial band, a resulting well-marked SSS freshening (~−1) near the dateline, and a SSS increase (~+1) below the mean position of the South Pacific Convergence Zone (SPCZ). The CP El Niño events are characterized by smaller (50%) eastward displacements of the eastern edge, a ~15° longitude westward shift of the equatorial SSS freshening, and a comparatively reduced (~50%) SSS increase in the SPCZ. A qualitative analysis indicates that changes in zonal currents and precipitation can account for the observed contrasted signature in SSS. Eastward current anomalies appear over most of the equatorial band during EP El Niño events. In contrast, there is a tendency for zonal current convergence slightly west of the dateline during CP El Niño events, consistent with the confinement of the warm/fresh pool in the western central equatorial basin, the related quasi-inexistent northeastward migration of the SPCZ, and associated heavy precipitation regime.

Citation: Singh, A., T. Delcroix, and S. Cravatte (2011), Contrasting the flavors of El Niño-Southern Oscillation using sea surface salinity observations, *J. Geophys. Res.*, *116*, C06016, doi:10.1029/2010JC006862.

1. Introduction

[2] The El Niño-Southern Oscillation (ENSO) phenomenon is the strongest climatic signal on an interannual time scale and greatly affects the world population [*Goddard and Dilley*, 2005; *McPhaden et al.*, 2006]. The ENSO comprises warm (El Niño) and cold (La Niña) episodes, with a returning time scale ranging from 2 to 7 years. The main properties of these two episodes are sometimes described as being negatively related, to the first order, but more interestingly, the properties differ within each episode. This was especially studied for the El Niño episodes which, at least, can vary in terms of phasing with the seasonal cycle [e.g., *Jin et al.*, 1994], strength [e.g., *Wolter and Timlin*, 1998], duration [e.g., *Glantz et al.*, 1991], onset time [e.g., *Wang*, 1995], and eastward or westward displacement of sea surface temperature (SST) anomalies along the equator [e.g., *Wang*, 1995; *McPhaden and Zhang*, 2009]. The recent detection of a "new type" of El Niño, termed as "Dateline El Niño" [*Larkin and Harrison*, 2005a], "El Niño Modoki" [*Ashok et al.*, 2007], "Warm Pool El Niño" [*Kug et al.*, 2009] or "central Pacific El Niño" [*Kao and Yu*, 2009], and hereafter referred to as the CP El Niño, has added a new dimension to the ENSO climatic puzzle. During this new type of El Niño, the maximum SST Anomalies (SSTA) are confined in the central equatorial Pacific, in contrast with the variously called "traditional," "canonical," "conventional," "cold tongue" or "eastern Pacific" El Niño (hereafter referred to as the EP El Niño), when they occur in the eastern Pacific. Interestingly, the CP El Niño has been shown to be more intense in recent years [*Lee and McPhaden*, 2010], and could be more frequent in a warming climate [*Yeh et al.*, 2009].

[3] Different methods and numerous indices have been used to document the occurrence and diversity of ENSO, and to classify the different types of El Niño. Perhaps the most commonly used indices to document ENSO are the atmospheric Southern Oscillation Index (SOI) and the oceanic Niño-1+2, Niño-3, Niño-3.4 and Niño-4 SST indices [e.g., *Rasmusson and Carpenter*, 1982; *Trenberth*, 1984, 1997]. Other indices have also been developed for specific process studies [e.g., *Delcroix*, 1998; *Leloup et al.*, 2007; *Meyers et al.*, 2007; *Wolter and Timlin*, 1998]. Most of these indices vary *rather* consistently with each other, as detailed

[1]IRD/LEGOS, UMR 5566, Toulouse, France.

0148-0227/11/2010JC006862

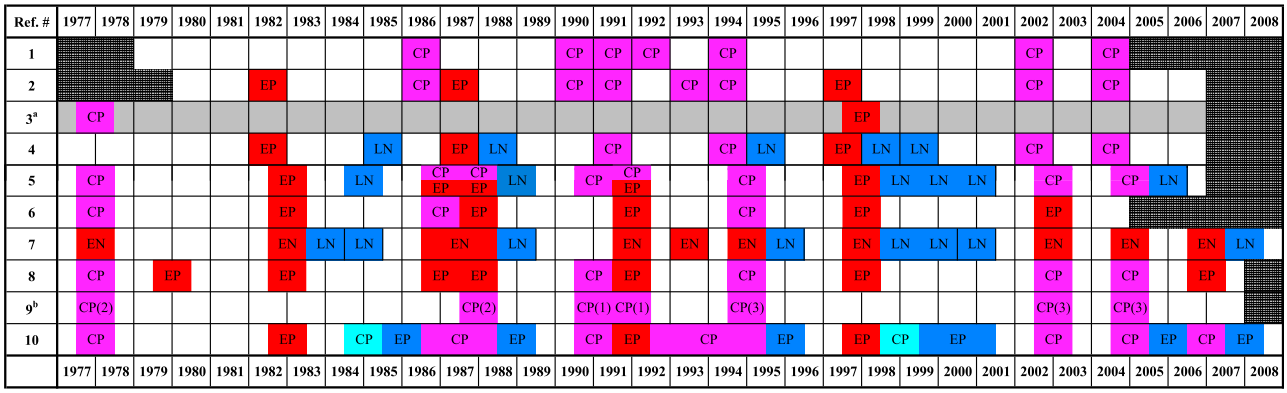

1	*Ashok et al.*, 2007	DJF SST composites; **CPEN**: EMI ≥ 0.7 of seasonal DJF standard deviation
2	*Hendon et al.*, 2009	SON SST composites; **EPEN**: Niño-3.4 > 1 standard deviation; **CPEN**: EMI > 0.7 standard deviation
3	*Kao and Yu*, 2009	**EPEN**: SST PC1 > 1 standard deviation (3 consecutive months); **CPEN**: SST PC2 > 1 standard deviation (3 consecutive months)
4	*Kim et al.*, 2009	ASO SST composites; **EPEN**: Niño-3 > 1 standard deviation; **CPEN**: Niño-4 > 1 standard deviation and Niño-3 < 1 standard deviation; **LN**: Niño-3 or Niño-3.4 < 1 standard deviation
5	*Kug et al.*, 2009	SONDJF SST composites; **EPEN**: Niño-3 > 1 standard deviation and standardized Niño-3 > standardized Niño-4; **CPEN**: N4 > 1 standard deviation and standardized Niño-4 > standardized Niño-3; **LN**: Niño-3 or Niño-4 < 1 standard deviation
6	*Larkin and Harrison*, 2005a,b	SONDJF SST composites; **EPEN**: Widely accepted years; **CPEN**: NOAA CPC definition
7	*World Meteorological Organization*	**EN**: ONI[c] > +0.5°C (5 consecutive months); **LN**: ONI < -0.5°C (5 consecutive months)
8	*Yeh et al.*, 2009	DJF SST composites (detrended for each decade from 1930); **EPEN**: Niño-3 > Niño-4; **CPEN**: Niño-4 > Niño-3
9	*Yu and Kim*, 2010	SONDJF SST composites; **CPEN**: CP index (*Kao and Yu*, 2009) > 1 standard deviation
10	Present results	From SSS clustering

Figure 1. Years of eastern Pacific (EP) and central Pacific (CP) El Niño (EN) (in red and pink) and La Niña (LN) (in blue and turquoise) events as defined by the various references and their criteria (at the bottom image). Dark hatched boxes show that the period was not analyzed by the respective authors. Light hatched boxes show that the period was analyzed but the authors did not classify the events. The acronym DJF stands for December-January-February, etc. The superscript a means these authors only classified two events as examples of EPEN and CPEN events. Further analysis from their work was done by *Yu and Kim* [2010]. The superscript b means only CPEN events were analyzed and subsequently divided into three classes. The superscript c means ONI is the World Meteorological Organization defined Oceanic Niño Index, which is defined as the 3 month running means of SSTA in the Niño-3.4 region.

for a few of them by *Deser and Wallace* [1987] and *Hanley et al.* [2003]. Yet, as a useful reference, the World Meteorological Organization (WMO), in 2005, has adopted a definition of El Niño and La Niña events based on the analysis of Niño-3.4 SSTA. The WMO years of the 1977–2008 events are given in Figure 1. In addition, to classify the different types of ENSO, new SST-based indices have been proposed recently to characterize the CP El Niño, including the Trans-Niño Index (TNI) [*Trenberth and Stepaniak*, 2001], El Niño Modoki Index (EMI) [*Ashok et al.*, 2007] and CP Index [*Kao and Yu*, 2009]. Depending on the method and SST-based index used, the years identified as EP or CP El Niño may slightly differ, as summarized in Figure 1.

[4] Studies have shown that different ENSO episodes, including EP and CP El Niño events, have different impacts on weather and climate, at both global and regional scales [*Larkin and Harrison*, 2005b; *Weng et al.*, 2007; *Ashok et al.*, 2009a, 2009b; *Cai and Cowan*, 2009; *Hendon et al.*, 2009; *Kim et al.*, 2009; *Vincent et al.*, 2009; *Yeh et al.*, 2009; *Chen and Tam*, 2010]. Most of them have used SST to stress the differences between ENSO episodes since the climatic impacts are sensitive to details of the surface warming (or cooling) of the equatorial Pacific [*Palmer and Mansfield*, 1984] via varying teleconnections, and because SST is by far the best observed oceanic variable. Interestingly, some of them have used variables other than SST involved in the ENSO cycle. For example, looking at recent publications only, *Bosc and Delcroix* [2008] and *Kug et al.* [2009] used sea level anomalies (SLA) as an alias for warm water volume (WWV) to differentiate between ENSO events, *Kao and Yu* [2009] identified the anomalous surface wind stress and vertical temperature structure associated with the EP and CP types of El Niño, *Yeh et al.* [2009] and *Kug et al.* [2009] found different signatures in precipitation anomalies during EP and CP El Niño events, while *Chiodi and Harrison* [2010] used outgoing longwave radiation (OLR) in the equatorial Pacific to distinguish between El Niño events.

[5] Using different variables to document ENSO clearly gives different perspectives rather than using SST only to understand its behavior, impacts and how it works. An

essential variable of the global climate observing system [*Global Climate Observing System*, 2004; see also *Lagerloef et al.*, 2008] that is also affected by the ENSO cycle is sea surface salinity (SSS). Indeed, precipitation patterns and heat fluxes are modified in the course of an El Niño or La Niña, affecting SSS. Moreover, anomalous surface currents have been simulated during CP El Niño [*Kug et al.*, 2009], and we can expect these currents to imprint on the distribution of SSS given the main role of zonal salt advection in the equatorial band at the ENSO time scale [*Picaut et al.*, 2001]. Hence, as a complement to previous studies, the goal of this paper is, for the first time, to contrast and tentatively explain the different flavors of ENSO using SSS.

[6] The rest of the paper is organized as follows. Section 2 describes the data and methodology. Section 3 recalls the mean structures for SST, SSS, precipitation (P) and zonal currents (U). Section 4 sets the context regarding EP and CP ENSO based on an Empirical Orthogonal Function (EOF) analysis on SST and then analyzes the ENSO-related SSS variability with an EOF analysis, Agglomerative Hierarchical Clustering (AHC), and representative examples of ENSO events. Section 5 discusses the main mechanisms likely responsible for observed ENSO-related SSS variations. Section 6 summarizes and discusses the findings of this study.

2. Data Sets and Methodology

[7] The SSS data were obtained from the 1° longitude by 1° latitude and 1 month gridded product of *Delcroix et al.* [2011] for the tropical Pacific region (30°S–30°N, 120°E–70°W) and from 1950 to 2008. This product is derived from data originating from Voluntary Observing Ships, TAO/TRITON moorings, CTD and Argo profilers. As the SSS coverage data is greatly time dependant, each grid point has an associated error indicating the confidence we can have on the SSS product at one particular month. This error is given as a percentage of the interannual variance at that point. When there is no SSS data available, the error is 100% and the SSS gridded value is equal to the monthly climatological SSS. In our analyses, we wish to exclude the grid points where too few data are available, and we consider somewhat arbitrarily that we can trust the SSS gridded product value if the error is less than the 80% threshold. In their analysis with a similar product, *Cravatte et al.* [2009] used an arbitrary value of 60% to define the error threshold. Initial sensitivity studies found that using 60% or 80% as the error threshold did not significantly change our results. Accordingly, regions where the mean error is less than 80% as well as data starting from 1977 only (due to poor data coverage before the mid 1970s) were used in our analysis. For SST, we chose to use the Met Office Hadley Centre for Climate Prediction and Research sea ice and sea surface temperature data set 1 (HadISST1) [*Rayner et al.*, 2003], available monthly from 1870 until present and with the same grid size as the SSS product. The Extended Reconstructed Sea Surface Temperature (ERSST) [*Smith and Reynolds*, 2003] and Kaplan [*Kaplan et al.*, 1998] data sets were also tested in addition to the HadISST1 product, and we found that there is not much difference in the end results for the low-frequency variations. We restricted the spatial and temporal domain for the SST data to be the same as that for the SSS data.

[8] The precipitation data used is from the Global Precipitation Climatology Project (GPCP) version 2.1 combined precipitation data set [*Huffman et al.*, 2009] of monthly means from combined satellite and station data on a 2.5° grid that is available from 1979 to present. This product is regridded on a 1° grid using triangle-based linear interpolation based on a Delaunay triangulation [*Barber et al.*, 1996] and constrained to the tropical Pacific region. We also tested the NCEP/NCAR Reanalysis 1 precipitation product [*Kalnay et al.*, 1996] available from 1948, and while there are not significant differences between the two products, we selected to show results from GPCP for our specified region because no precipitation observations are assimilated in the reanalysis product [*Janowiak et al.*, 1998]. The surface (0–30 m) currents are derived from the Ocean Surface Currents Analyses-Real time (OSCAR) product, which is available on a 1° grid monthly from October 1992 [*Bonjean and Lagerloef*, 2002]. We also tested the Centre of Topography of the Oceans and the Hydrosphere (CTOH) [*Sudre and Morrow*, 2008] and Archiving, Validation and Interpretation of Satellite Oceanographic data (AVISO) surface currents products and got basically the same results as with the OSCAR product. The Websites for downloading all the gridded fields we used are given below in the Acknowledgments paragraph.

[9] All data sets were detrended (except for the zonal currents as the time series are too short) over the 1977–2008 period for SSS and SST, and 1979–2008 for precipitation. This proved necessary as, for example, the freshening trend observed in the warm pool over the last 30 years [*Delcroix et al.*, 2007; *Cravatte et al.*, 2009] could have been (mis) interpreted as a sign of increased intensity or occurrence of El Niño events. Yet, it is also possible that part of the observed linear trends in SST and SSS in the central equatorial Pacific are due to an increase of El Niño intensity in the central Pacific, as suggested by *Lee and McPhaden* [2010] for SST and discussed in section 6 for SSS.

[10] A number of different data analysis procedures were then performed on the anomalies (relative to the mean monthly climatology) in order to characterize the different ENSO signatures. These include time filtering using different filter lengths, EOF analysis [e.g., *Emery and Thomson*, 2001], linear regressions of anomalies onto ENSO indices (e.g., Niño-1+2 and Niño-4 SSTA), combined regression-EOF analysis (as used by *Kao and Yu* [2009]), neural network analysis [*Kohonen*, 1989] and agglomerative hierarchical clustering (AHC) [*Kohonen*, 1989]. We choose to discuss results derived from the well-known EOF analysis and less frequently used AHC technique only. These two techniques were performed on 13 months Hanning filtered anomalies. This filter passes almost no signal at periods of 6 months and shorter and so looks appropriate since the duration of CP ENSO was found to be less than 1 year [e.g., *Ashok et al.*, 2007; *Weng et al.*, 2007; *Kao and Yu*, 2009].

[11] In the AHC procedure, each singleton (defined as a monthly anomaly map) is initially merged with another according to the smallest Euclidean distance between each pair of singletons. Each resulting merged cluster is then

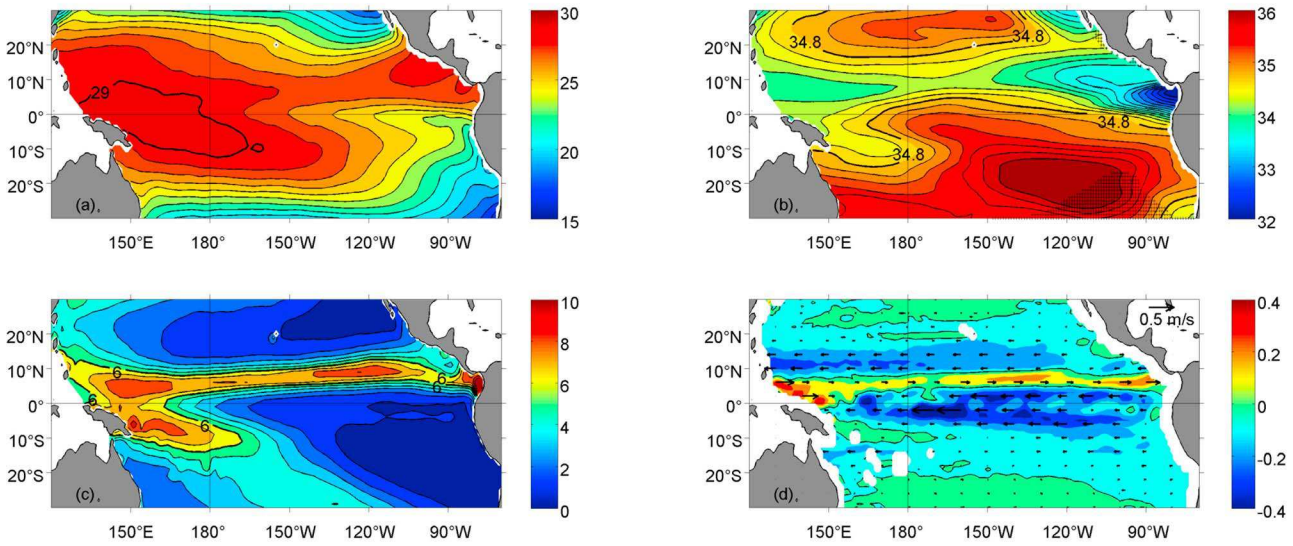

Figure 2. Mean structures of (a) SST, (b) SSS, (c) precipitation, and (d) zonal currents in the tropical Pacific region. The heavy contour lines in Figures 2a–2c represent the 29°C isotherm, 34.8 isohaline, and 6 mm d^{-1} isohyet, respectively. The contour spacing is 1°C, 0.2, and 1 mm d^{-1} in Figures 2a–2c, respectively. The regions shaded in black in the southeastern tropical Pacific in Figure 2b denote regions where the normalized error in SSS is larger than 80% and that are not used in the analysis. Positive values in Figure 2d denote eastward currents.

paired with another merged cluster according to the *Ward* [1963] criterion (which is analogous to the Euclidean distance for singletons). This procedure was repeated until the remaining two clusters were finally merged into the complete data set. The clustering procedure can be represented by a dendrogram, which illustrates the fusions made at each successive step of the analysis and the linkage (separation) distance between each successive clustering. Further examples on the use of the above clustering technique can be found in the work by *Kao and Yu* [2009] and *Vincent et al.* [2009].

3. Mean Structures

[12] The mean structures for SST, SSS, precipitation and zonal currents fields are first reminded in Figure 2. For SST, the presence of a smooth temperature gradient along the equatorial region distinguishes the warm pool (characterized here by SST greater than 29°C) in the west from the equatorial upwelling region in the east. High SST bands are found along the Inter Tropical Convergence Zone (ITCZ) north of the equator and in the South Pacific Convergence Zone (SPCZ), which is obliquely oriented along the northwest-southeast axis in the southwest tropical Pacific. The poleward decrease in SST is evident from ~15°–20° latitude. The mean SSS structure shows low-salinity waters observed under the ITCZ and SPCZ and in the western equatorial Pacific. A strong minimum in SSS is also observed in the far eastern Pacific within 5°N–10°N, south of the eastern warm pool. Two high-salinity cores are found northwest of Hawaii and in the vicinity of Tahiti. In the equatorial region, SSS increases westward from the Americas to the central Pacific and then decreases farther to the west, with the 34.8 isohaline lying close to the eastern edge of the warm pool. High precipitation (>6 mm d^{-1}) is found in the ITCZ and SPCZ regions, which are linked together in the western Pacific just north of the equator in the warm pool area. Regions deficient in precipitation are observed in the northeastern and southeastern tropical Pacific. For zonal currents, the westward flowing north equatorial current (NEC) and south equatorial current (SEC) are most evident in the 10°N–15°N and 10°S–5°N bands with maximum magnitudes around 0.30 m s^{-1} and 0.55 m s^{-1}, respectively. The eastward flowing north equatorial counter current (NECC) lies in the 5°N–10°N band with maximum amplitudes close to 0.47 m s^{-1}. Its much weaker (maximum amplitude of 0.1 m s^{-1}) southern counterpart, the South Equatorial Counter Current (SECC) is also visible at around 10°S–5°S, east of the Solomon Islands.

4. SST and SSS Signal During ENSO

4.1. EOF Analysis

[13] To set the context, especially regarding the signature of EP and CP ENSO, Figures 3 and 4 show the results of an EOF analysis performed on 13 months Hanning filtered SST and SSS anomalies. The first EOF on SST accounts for 56.9% of the interannual variance. The spatial pattern (Figure 3) shows anomalous SST warming off the South American coast extending toward the central Pacific along the equatorial region. Its time function (SST-PC1) is highly correlated with the 13 months Hanning filtered SOI (R = −0.91; SOI leading by 1 month). The second EOF on SST accounts for 13.6% of the interannual variance. The spatial

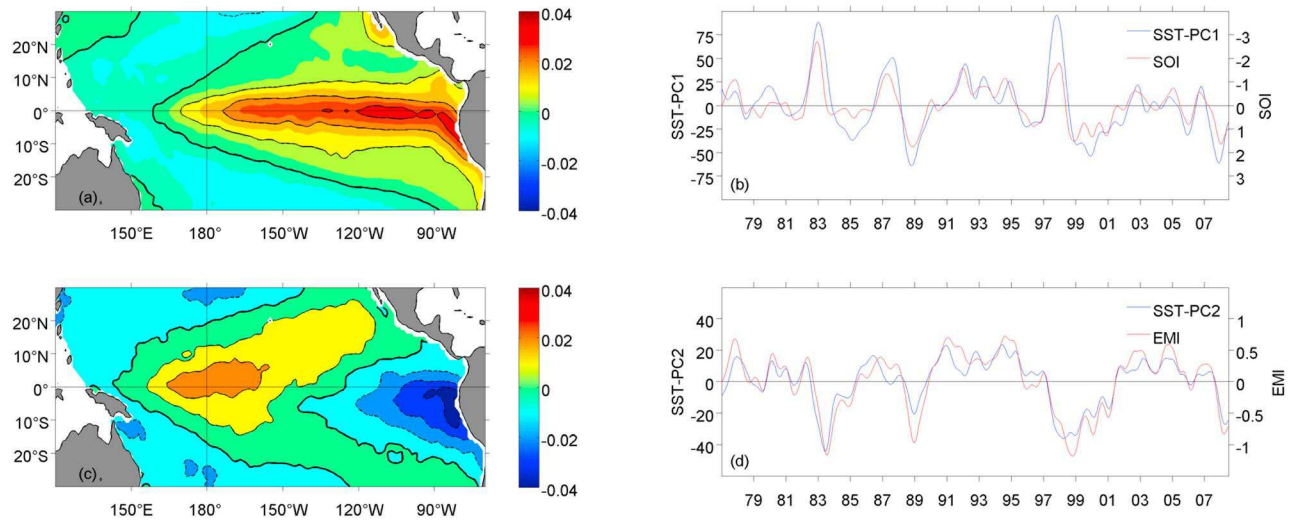

Figure 3. Spatial structures for (a) EOF1 and (c) EOF2 and (b and d) their corresponding time functions (in blue) for the first and second modes of the EOF on SSTA, respectively. The units are defined so that the product between the spatial pattern and the corresponding time function denotes degree Celsius. Note the different vertical scales for the time functions. The red lines in the time functions denote the 13 months Hanning filtered SOI (in Figure 3b) and EMI (in Figure 3d), scaled on the right vertical axis. Note the reversed vertical scale for the SOI.

pattern shows a large meridional "horseshoe pattern" of warm SSTA in the central Pacific region flanked by cold SSTA in the eastern equatorial Pacific and, to a lesser extent, in the far western basin. Its time function (SST-PC2) shows high correlation with the 13 months Hanning filtered EMI (R = 0.94; SST-PC2 leading by 1 month), noting that the variations in SST EOF2 are about half of those from SST EOF1. Note that the EMI is defined as: $[SSTA]_A - (0.5 \times ([SSTA]_B + [SSTA]_C))$, where the square brackets represent the area averaged SST anomalies over the regions A (165°E–140°W, 10°S–10°N), B (110°W–70°W, 15°S–5°N) and C (125°E–145°E, 10°S–20°N) [*Ashok et al.*, 2007]. According to *Ashok et al.* [2007], the spatial patterns of SST EOF1 and EOF2 associated with the positive phase of their time functions are characteristic of EP and CP El Niño, respectively.

[14] The first EOF for SSS accounts for 28.6% of the interannual variance. The spatial pattern (Figure 4) shows negative loadings in the western central equatorial Pacific region with maximum values west of the dateline (up to 0.043), and positive loadings with maxima (around 0.036) found further south in the SPCZ region. Its time function (SSS-PC1) is highly correlated with SST-PC1 (R = 0.91; SST-PC1 leading by 3 months). Negative (positive) loadings in Figure 4a thus indicate a decrease (increase) of SSS during El Niño events, and vice versa during La Niña events. These SSS EOF1 results are in agreement with those of *Delcroix* [1998] who found similar patterns using data from 1976 to 1992 only, though our confidence is strengthened in the present analysis in which we double the record length. By analogy with SST EOF1, it is tempting to conclude that this SSS EOF1 characterizes the SSS signature of EP ENSO. The second and third SSS EOFs extract a total of 25.6% (13.2 + 12.4) and are not shown here. Although their time functions are well correlated with SST-PC2 (R = 0.44 and R = 0.75) at zero lag, a simple test of significance

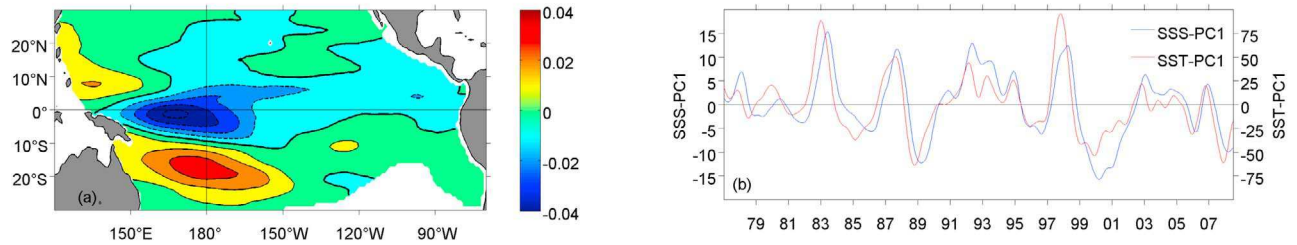

Figure 4. (a) Spatial structure and (b) corresponding time function (in blue) for the first mode of the EOF on SSSA. The red line in the time function denotes SST-PC1, as in Figure 3b, scaled on the right vertical axis. The white areas in the southeastern tropical Pacific in Figure 4a denote regions where the normalized error in SSS is larger than 80% and are not used in the analysis.

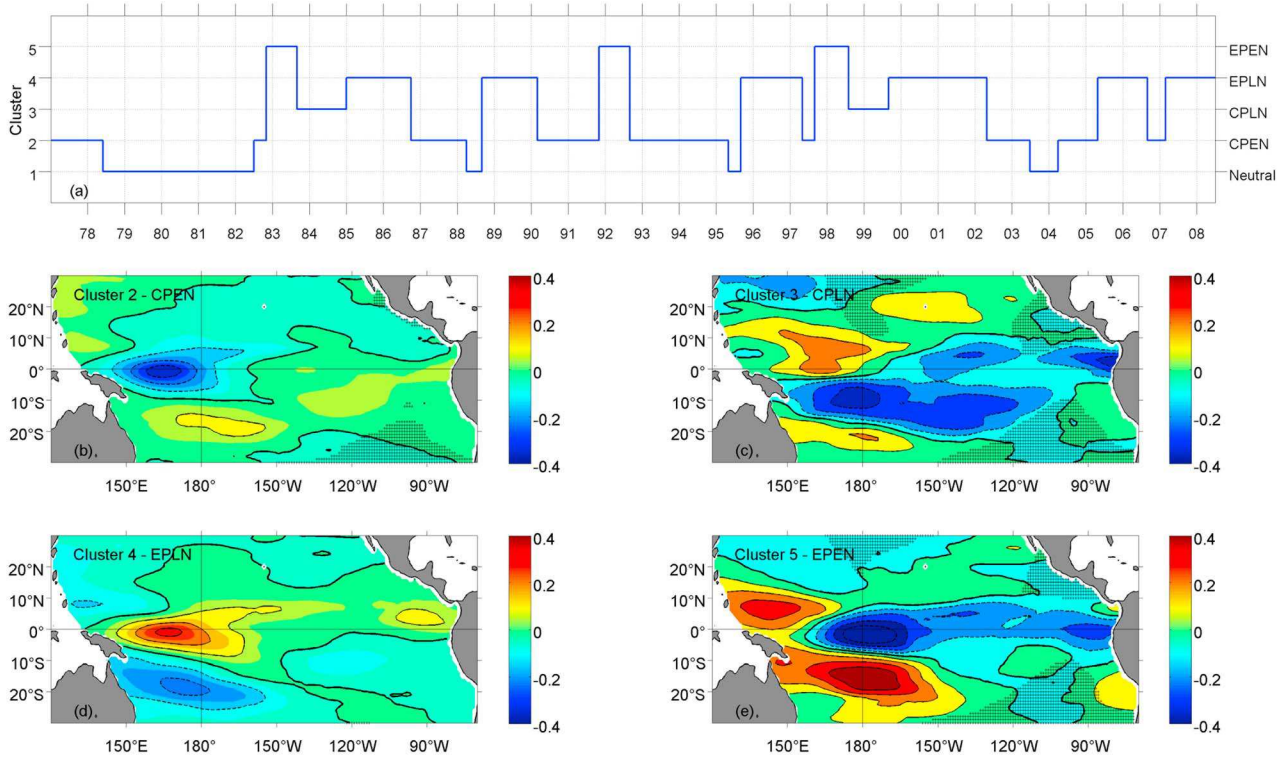

Figure 5. (a) The cluster time series shows which cluster best represents the SSSA pattern at a particular time. The abscissa labels denote the beginning of the year. Spatial structures from the agglomerative hierarchical clustering technique on SSSA with (b) cluster 2 showing CP El Niño conditions, (c) cluster 3 showing CP La Niña conditions, (d) cluster 4 showing EP La Niña conditions, and (e) cluster 5 showing EP El Niño conditions. The regions shaded in black, mainly located in the southeastern tropical Pacific, denote regions where the normalized error in SSS is larger than 80%.

[*North et al.*, 1982] applied to the eigenvalues shows that these EOFs cannot be distinguished in a statistically significant way and thus probably do not extract (or extract a mixture of) real physical phenomena.

4.2. AHC Analysis

[15] The advantage of the above EOF analysis is that it provides a compact description of the spatial and temporal variability of SST and SSS. Noteworthy, it implicitly assumes symmetry in the spatial patterns of the El Niño and La Niña events denoted by the positive and negative phases of the EOF time functions, respectively. As discussed in a few papers [e.g., *Larkin and Harrison*, 2002] and in the following paragraphs, the El Niño and La Niña spatial patterns are however not strictly symmetrical. Moreover, the EOF analysis on SSS suggests that the CP ENSO signal is likely spread, at least, over the second and third EOF modes. Given these EOF limitations, an AHC analysis was performed on the low-pass filtered monthly SSS Anomaly (SSSA) maps in an attempt to better discriminate the signature of EP and CP ENSO in SSS.

[16] The AHC technique was found to be rather sensitive to the selected SSS data coverage and data processing. Hence, we show only robust clusters that appear whatever the used error thresholds (tested from 60% to 80%), spatial coverage (from 20°S–10°N to 30°S–30°N and 120°E–70°W), and low-pass filter lengths (from 13 to 25 months). Five clusters for a total of 379 maps were identified at the top of the dendrogram tree (not shown here) using 80% as the maximum SSS error and 13 months Hanning filtered SSSA maps in the region 20°S–10°N, 120°E–70°W. As discussed below, the five clusters characterize the neutral, EP and CP El Niño and EP and CP La Niña conditions, and occur approximately 18%, 8%, 34%, 33% and 8% of the time, respectively.

[17] The cluster time series together with the cluster maps in terms of SSS are shown in Figure 5. The spatial pattern of the fourth cluster (Figure 5d) shows high positive SSS anomalies (maximum of 0.33) located mostly west of the dateline in the equatorial region and a strong freshening (maximum of 0.23) located south of the mean SPCZ position. The timing of that cluster 4 (1985–1986, 1988–1989, 1995–1996, 1999–2001, 2005–2006 and 2007–2008) indicates that this pattern characterizes the EP La Niña signal in SSS (according to SST-PC1). The spatial pattern of cluster 1 (not shown here) is somewhat similar to cluster 4 with smaller SSS anomalies, and occurs during periods when the ENSO signal is the weakest (also according to SST-PC1 and SST-PC2). Similarities between clusters 1 and 4 thus suggest that this cluster is characteristic of neutral conditions, and that the La Niña situation could be interpreted simply as an enhanced neutral situation [e.g., *Meyers et al.*, 2007]. The pattern in cluster 5 (Figure 5e) roughly shows opposite signs to the pattern in clusters 1 or 4. Its timing represents the very

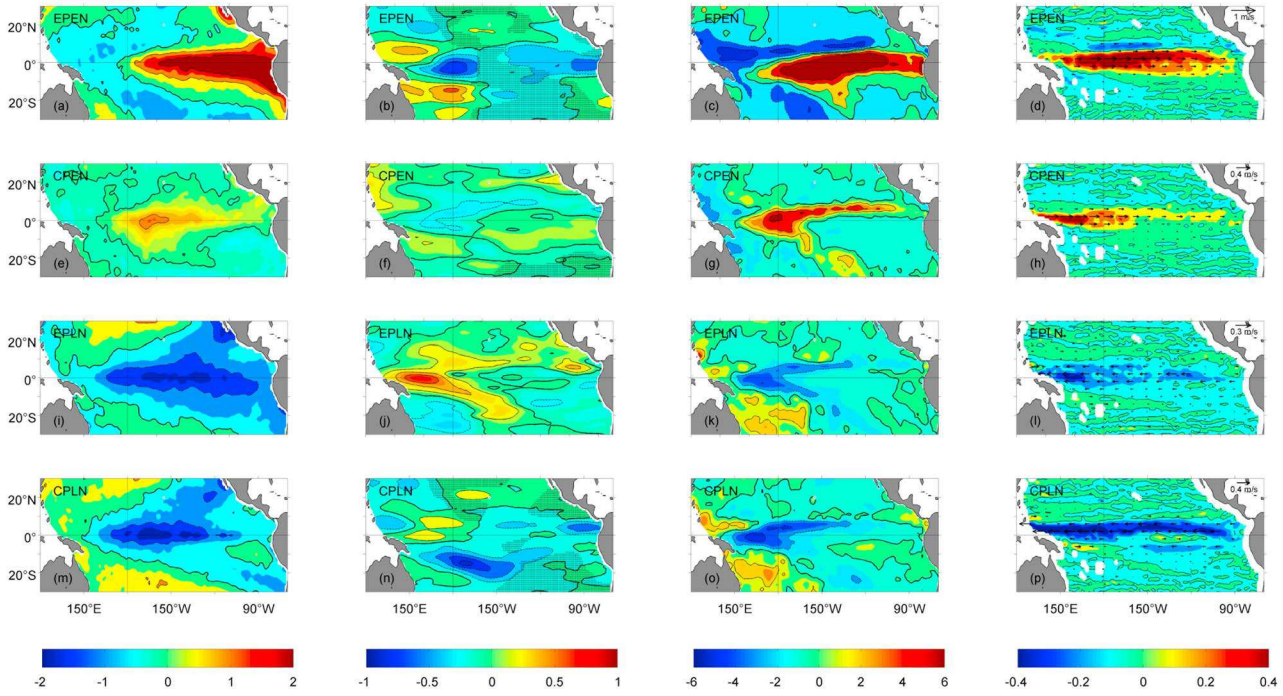

Figure 6. Three monthly DJF averages of SSTA (first column), SSSA at 3 months lag (second column), precipitation anomalies at zero lag (third column), and zonal currents anomalies at 3 months lead (fourth column) for the (a-d) 1997–1998 EP El Niño, (e-h) 2002–2003 CP El Niño, (i-l) 2007–2008 EP La Niña, and (m-p) 1998–1999 CP La Niña. The regions shaded in black in the second column denote regions where the normalized error in SSS is larger than 80%. Units are as in Figure 2.

strong 1982–1983 and 1997–1998 and strong 1991–1992 EP El Niño events, thus we conclude that this cluster extracts the EP El Niño signal. Interestingly, these three events correspond to the only El Niño events associated with the occurrence of deep atmospheric convection (OLR < 230 W m^{-2}) lasting at least half a year in the central equatorial Pacific [*Chiodi and Harrison*, 2010]. The maximum negative SSS anomalies (0.51) for these events are centered close to the equator and the dateline, and high-salinity cores are found in the SPCZ region and north of Papua New Guinea with maximum amplitudes of 0.51 and 0.35, respectively. Cluster 3 (Figure 5c) shows negative SSS anomalies zonally oriented over the SPCZ region (maximum of 0.37) and sandwiched between two positive anomaly regions: one centered west of the dateline in the equatorial region (maximum of 0.29) and the other approximately between 30°S and 20°S (maximum of 0.21). In the equatorial region, higher salinities are confined west of ~165°W while lower salinities are evident to extend southeastward from the SPCZ region. The timing of this cluster occurs during 1983–1984 and 1998–1999, after the two very strong EP El Niños in 1982–1983 and 1997–1998 (consistent with findings by *Yu et al.* [2010b]) and before the EP La Niña events of 1985–1986 and 1999–2001, respectively, and thus this cluster represents the CP La Niña signal in SSS. A reduction in the amplitudes of the SSS anomalies is seen in cluster 2 (Figure 5b), as compared to the EP El Niño in cluster 5 (Figure 5e), especially in the SPCZ region (maximum of 0.36) and with a ~15° westward displacement of the low-salinity core in equatorial region as compared to cluster 5. The timing of cluster 2 coincides with those of CP El Niño events in 1977–1978, 1986–1988, 1990–1991, 1992–1995, 2002–2003, 2004–2005 and 2006–2007, according to the dates of positive values of SST-PC2 or EMI in Figure 3. Interestingly, the frequency of CP El Niño (cluster 2) does not increase significantly with time during the 30 year period from 1977 to 2008 (e.g., in Figure 5a, 16% and 17% of CP El Niño events occurred in the first and second halves of that period, respectively), as could occur under global warming as suggested by *Yeh et al.* [2009] and *Lee and McPhaden* [2010] using SST. Note, however, that the few numbers of sampled EP and CP El Niño events prevents us to be firmly conclusive in this matter.

4.3. Representative Examples

[18] To further help reduce the possibility that the SSS patterns in Figures 4 and 5 are artificial results of the statistical EOF and AHC analyses, the two left columns in Figure 6 shows DJF (December to the following February) composites of SSTA, and MAM (March-April-May) composites for SSS anomalies for the 1997–1998 EP El Niño, 2002–2003 CP El Niño, 2007–2008 EP La Niña and 1998–1999 CP La Niña events. The 3 months SST/SSS lag has been estimated from the EOF analysis in Figures 3 and 4, as well as from a visual detection of the peak anomalies on monthly mean maps. Reassuringly, these four presented examples, as well as others not shown here, are quite consistent with the AHC analysis. The remaining subtle differences between each example and its corresponding ENSO type in the AHC analysis, however, remind us of the

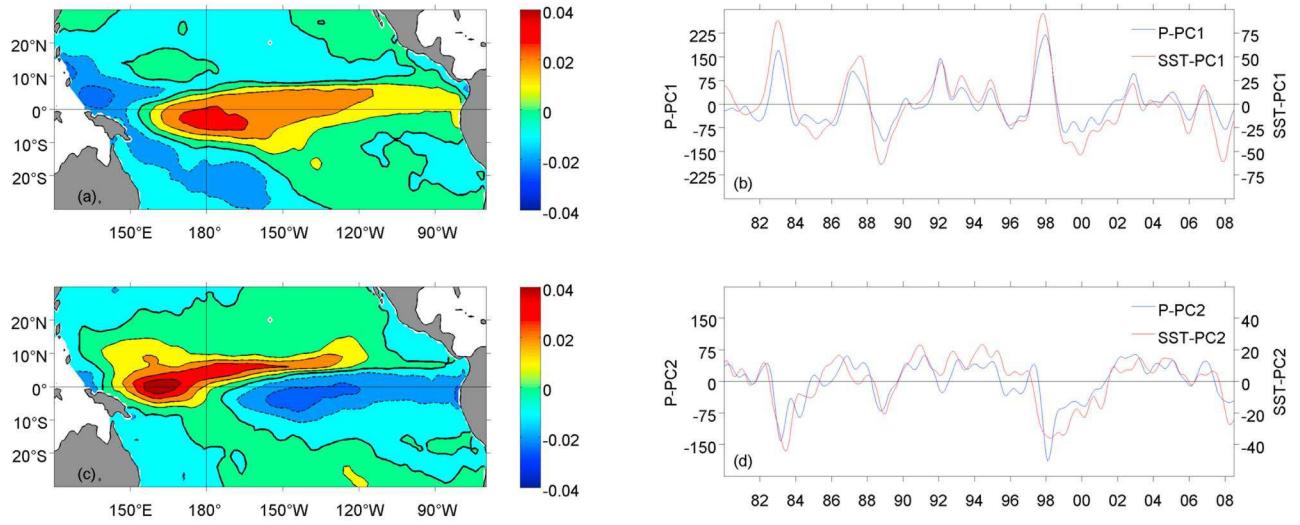

Figure 7. (a-d) Same as Figure 3 but for the precipitation anomalies. The units are defined so that the product between the spatial pattern and the corresponding time function denotes mm d^{-1}. Note the different vertical scales for the time functions. The red lines in the time functions denote SST-PC1 (in Figure 7b) and SST-PC2 (in Figure 7d), scaled on the right vertical axis.

uniqueness of each individual event, at least in terms of SST and SSS. In addition, these examples confirm, if needed, that the SST and SSS spatial patterns are not quite symmetrical during the El Niño and La Niña events (e.g., compare Figures 6a and 6i and Figures 6b and 6j).

5. Proposing Mechanisms Responsible for Contrasted ENSO-Related SSS Changes

[19] The contrasted ENSO signals observed in SSS result from the different contributions of terms involved in the salt conservation equation in the salinity mixed layer. These terms, however, cannot be quantitatively computed with confidence using observational data. Hence, as an alternative approach, this section qualitatively discusses how precipitation and zonal currents, the main two terms affecting SSS changes [e.g., *Picaut et al.*, 2001; *Gouriou and Delcroix*, 2002; *Vialard et al.*, 2002], might induce the observed contrasted signals. An EOF analysis on precipitation and zonal currents is first presented to get a general view, and we then focus on the equatorial region and SPCZ mean areas where the maximum ENSO-related SSS changes are observed. Statistical tests based on the work by *North et al.* [1982] indicate the presented EOF1 and EOF2 are well separated and are thus likely representative of real physical phenomena, as supported by the representative examples portrayed in the two right columns of Figure 6.

5.1. Precipitation and Zonal Currents Signal During ENSO

[20] The spatial patterns of P EOF1 (Figure 7a), which accounts for 39.9% of the total variance, shows positive loadings concentrated in the central equatorial Pacific region (between ~170°E and 165°W with maximum loadings of 0.037) and expanding to the east over the ITCZ region (~5°N). Negative loadings can be found in the far western equatorial Pacific (maximum of 0.025) and extending southeastward over the SPCZ region. The spatial pattern for P EOF2 (Figure 7c), showing 22.8% of the total variance, illustrates that the positive maximum loadings (0.046) in the equatorial region tend to be west of the dateline and ~15°–20° of longitude westward of the positive maximum loadings found in P EOF1. However, the tendency for the positive loadings to appear north of the equator still remains. Noteworthy, the negative loadings that were present over the SPCZ region in P EOF1 have disappeared in P EOF2. Negative loadings (maximum of 0.026) are found east of the dateline extending toward the South American coast along the equatorial region. The principal components of P EOF1 (P-PC1) and P EOF2 (P-PC2) show high positive correlations of R = 0.94 and R = 0.82 with SST-PC1 (at zero lag) and SST-PC2 (with P-PC2 leading by 1 month), respectively. This implies that the two P EOFs represent the EP and CP ENSO signals, respectively, with positive loadings in Figures 7a and 7c denoting enhanced precipitation during EP and CP El Niño events. As also noticed by *Larkin and Harrison* [2005b], the precipitation signature of EP and CP El Niño can thus be dramatically different for Pacific countries, especially in the southwestern tropical region where precipitation changes are much smaller during CP events, and in the central and eastern equatorial region where they are of opposite signs. Consistent results were derived by computing correlation coefficients between precipitation changes versus the principle components of the SST EOFs [*Kao and Yu*, 2009], and by making composites of individual events [*Kug et al.*, 2009] (also shown here in Figure 6).

[21] The time functions and spatial patterns of U EOF1 and U EOF2, which account for 48.6% and 11.4% of the variance, respectively, are shown in Figure 8 (recall that the zonal currents time series start in 1992 only). As was found above for precipitation, there are high correlations of U-PC1 and U-PC2 with SST-PC1 (R = 0.80; U-PC1 leading by

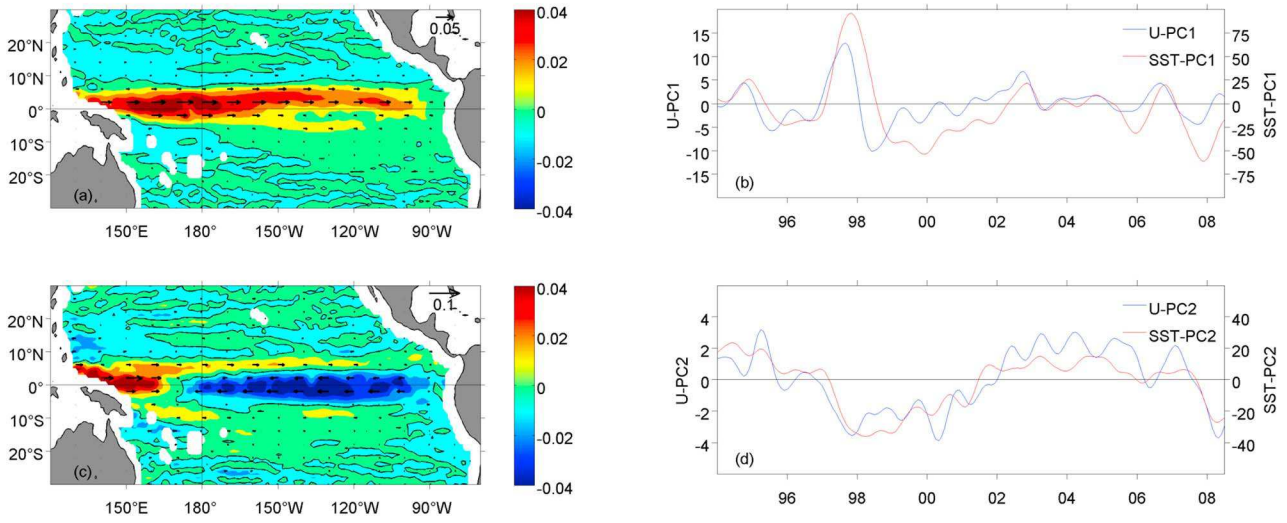

Figure 8. (a-d) Same as Figure 3 but for the surface zonal current anomalies. The units are defined so that the product between the spatial pattern and the corresponding time function denotes m s^{-1}, and positive values represent eastward current anomalies. The red lines in the time functions denote SST-PC1 (in Figure 8b) and SST-PC2 (in Figure 8d), scaled on the right vertical axis.

4 months) and SST-PC2 (R = 0.87; SST-PC2 leading by 1 month), respectively. This indicates that U EOF1 and U EOF2 are representative of the EP and CP ENSO signals, correspondingly. During EP El Niño, eastward current anomalies dominate most of the equatorial region, with a tendency for the maximum amplitudes to appear slightly north of the equator east of ~160°W. During CP El Niño, the eastward anomalies over the far western equatorial Pacific region remain with maximum loadings greater than 0.050 (as in U EOF1). There is, however, a reversal of the current anomalies east of about 160°E–170°E in the equatorial region (with maximum negative loadings of 0.046) so that the U EOF2 resembles the mean zonal currents field (Figure 2d). Such a reversal is crucial as it means a convergence of surface current anomalies near 175°E favoring the confinement of the warm and fresh pool in the western central basin as observed during CP El Niño [see also *Kug et al.*, 2009, Figure 9] (also shown here in Figure 6h). Away from the equatorial band, small eastward current anomalies tend to dominate in the NECC and over the entire south Pacific region.

[22] Generally, in the equatorial band, the EOF analysis suggests that for the EP El Niño (cluster 5 in Figure 5e), eastward equatorial zonal current anomalies bring in low-salinity waters from the far western equatorial Pacific into the central equatorial region. This combined with the high precipitation anomaly east of about 150°E, further lowers the salinity in this region, consistent with the findings of *Delcroix and Picaut* [1998]. For the CP El Niño (cluster 2 in Figure 5b), the low-salinity waters in the far western equatorial Pacific are consistent in space with the reduced zonal extension of anomalous eastward zonal currents and high precipitation. Similarly, the westward zonal current anomalies and rainfall deficit east of the dateline are in agreement with the higher salinity found in the region. In the SPCZ region, the precipitation deficit combined with the hint for small westward current anomalies in the western Pacific (due to the northeastward displacement of the SPCZ; see section 5.3) results in increased salinity during EP El Niño, as found by *Gouriou and Delcroix* [2002]. In contrast, weaker precipitation deficit and eastward current anomalies tend to dominate the entire Pacific region south of about 8°S during CP El Niño. As a result, higher than average salinity waters remain as during EP El Niño but with reduced magnitude due to the SPCZ position near its normal position (see section 5.3).

5.2. SSS Changes in the Equatorial Region

[23] In addition to the above EOF analyses, Figure 9 illustrates the tight relationships between the 2°S–2°N averaged SSS, precipitation and zonal currents over their respective measurement periods. The zonal displacements of the eastern edge of the warm pool, characterized by the 34.8 isohaline positions, agree well with both the zonal current direction and heavy precipitation location, corroborating earlier results obtained for different time periods [*Delcroix and Picaut*, 1998; *Picaut et al.*, 1996, 2001]. As expected from U EOF, Figure 9 also indicates that eastward current anomalies extend further to the east during the EP (1997–1998) than during the CP El Niño events (1992–1995, 2002–2003, 2004–2005 and 2006–2007), with CP El Niño events showing a current convergence in the western central basin.

[24] The 2°S–2°N averaged positions of the 34.8 isohaline for eleven El Niño and nine La Niña events of the years 1977–2008 are compared in Figures 10a and 10b, respectively. The mean position of the 34.8 isohaline (heavy black line) reaches its maximum eastward position (MEP) of ~175°W during November of the El Niño year, and its maximum westward position (MWP) of ~155°E during May of the La Niña year. During the EP El Niños, the MEP of the 34.8 isohaline is further east of the mean position. In con-

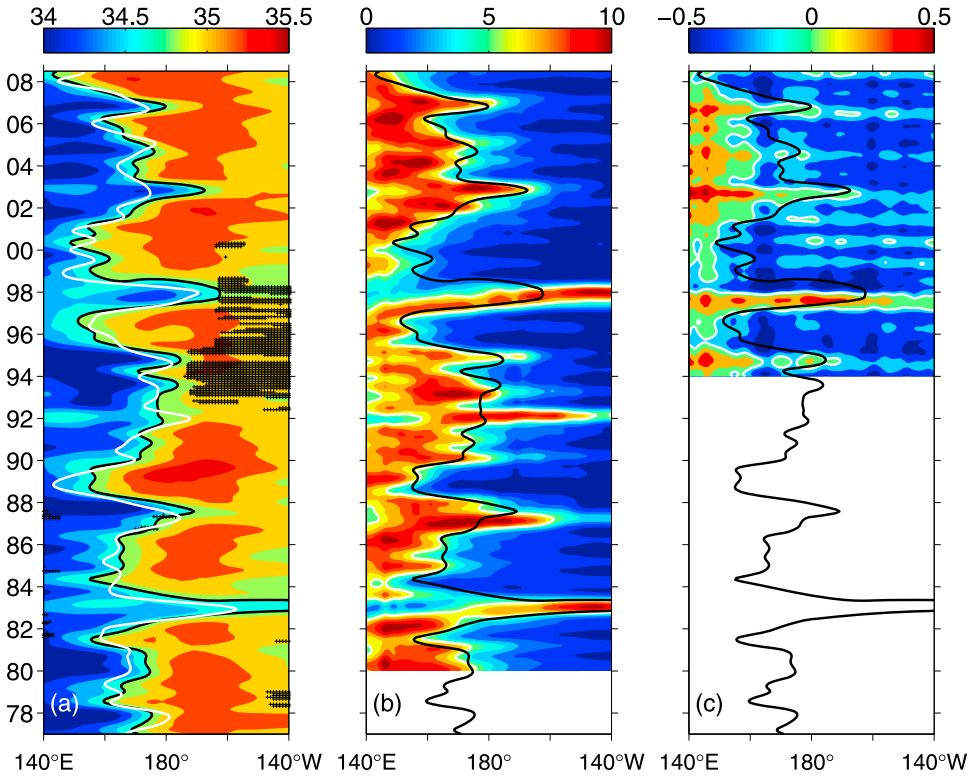

Figure 9. Time-longitude distribution of 2°S–2°N averaged (a) SSS, (b) precipitation, and (c) zonal currents showing the 34.8 isohaline position in continuous black, and overlaid in white are the SOI (in Figure 9a), 6 mm d^{-1} isohyet (in Figure 9b), and 0 m s^{-1} isotack (in Figure 9c).

trast, during CP El Niño, the MEP of the 34.8 isohaline lies west of the mean isohaline position. It is interesting to note that the timing of the MEP of the 34.8 isohaline generally occurs before the peak of the mean isohaline position during CP El Niño's in contrast to the EP El Niño's. The CP La Niña events generally peak before the EP La Niña events. In general, CP ENSO events peak earlier than EP ENSO events while the MEP (MWP) of the 34.8 isohaline show greater displacements from the mean isohaline position during EP rather than during CP El Niño (La Niña) events.

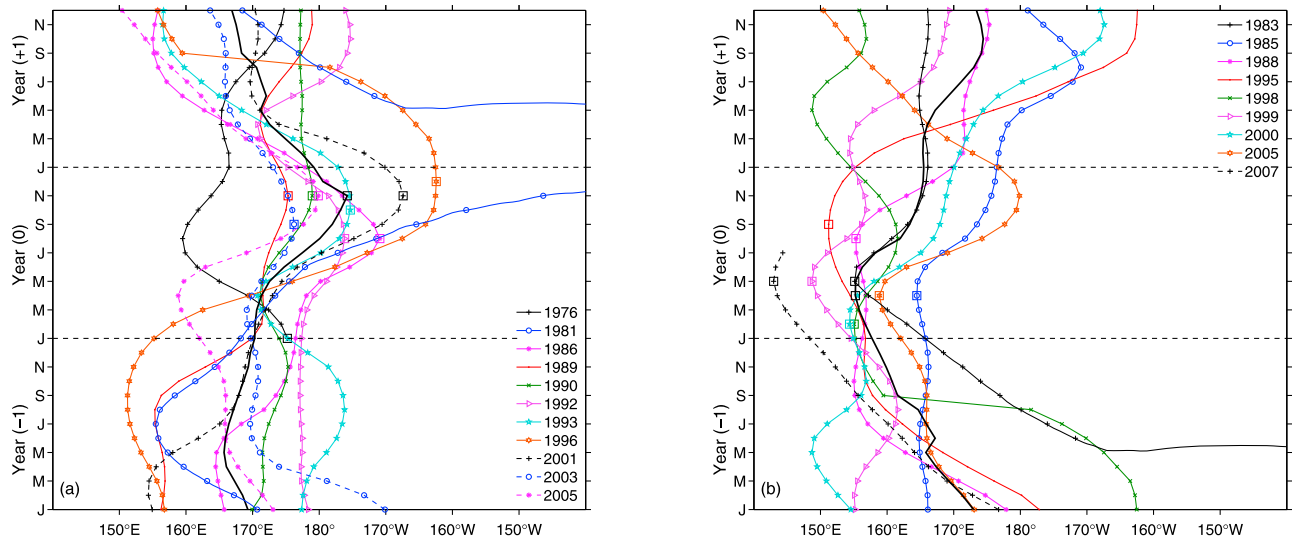

Figure 10. Zonal displacements of the 2°S–2°N averaged 34.8 isohaline position during (a) eleven El Niño events and (b) nine La Niña events. Year (0) represents the year of the peak El Niño/La Niña, and Year (−1) and Year (1) represent the year before and after, respectively. The years indicated in the legend correspond to Year (−1). The heavy black line shows the mean isohaline position for the eleven El Niño events in Figure 10a and nine La Niña events in Figure 10b.

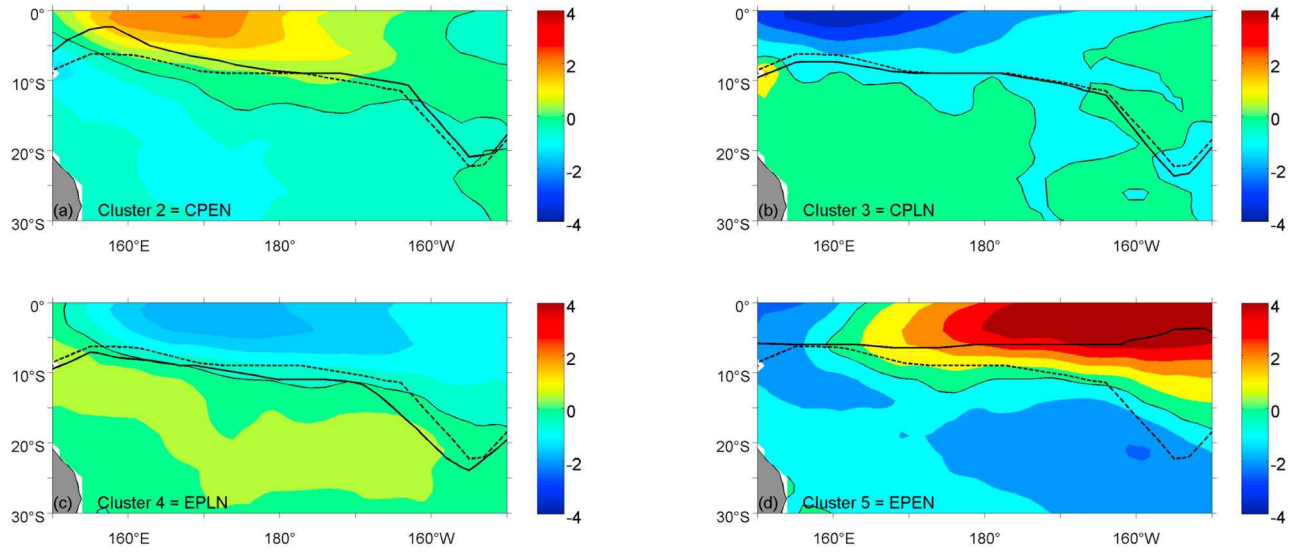

Figure 11. The spatial structures of the precipitation anomalies extracted from the SSS cluster time series in Figure 5 with precipitation leading by 3 months, (a) with cluster 2 showing CP El Niño conditions, (b) cluster 3 showing CP La Niña conditions, (c) cluster 4 showing EP La Niña conditions, and (d) cluster 5 showing EP El Niño conditions. Superimposed are the mean SPCZ positions estimating from precipitation data for the entire data length (dashed black line) and during the respective cluster timing (continuous black line).

5.3. SSS Changes in the SPCZ Region

[25] The correlation between EOF1 principal components of SSS and precipitation is maximum when precipitation is leading SSS by 3 months. Using this lag, we extracted the precipitation signal from the SSS cluster time series (Figure 5) for each cluster from 1980 to 2008 and averaged it (as was done to obtain the SSS clusters) for the southwestern tropical region (0°–30°S, 150°E–150°W). The mean position of the SPCZ for each cluster was then calculated by averaging the position of maximum precipitation for each map that makes up the cluster. The mean SPCZ position over the entire time series was calculated in a similar way. The resulting precipitation patterns corresponding to the SSS clusters are shown in Figure 11, together with the mean

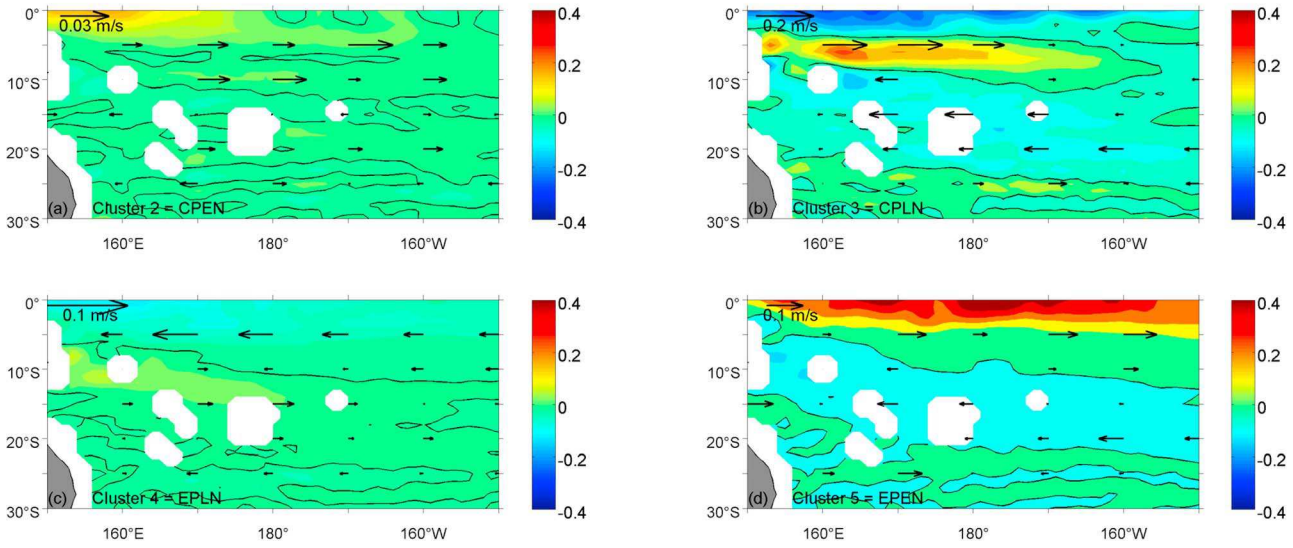

Figure 12. The spatial structures of the zonal currents anomalies extracted from the SSS cluster time series in Figure 5 with zonal currents leading by 7 months, with (a) cluster 2 showing CP El Niño conditions, (b) cluster 3 showing CP La Niña conditions, (c) cluster 4 showing EP La Niña conditions, and (d) cluster 5 showing EP El Niño conditions. Note the different scales for the zonal currents arrows: 0.03 m s^{-1} in Figure 12a, 0.2 m s^{-1} in Figure 12b, and 0.1 m s^{-1} in Figures 12c and 12d. Positive values denote eastward current anomalies.

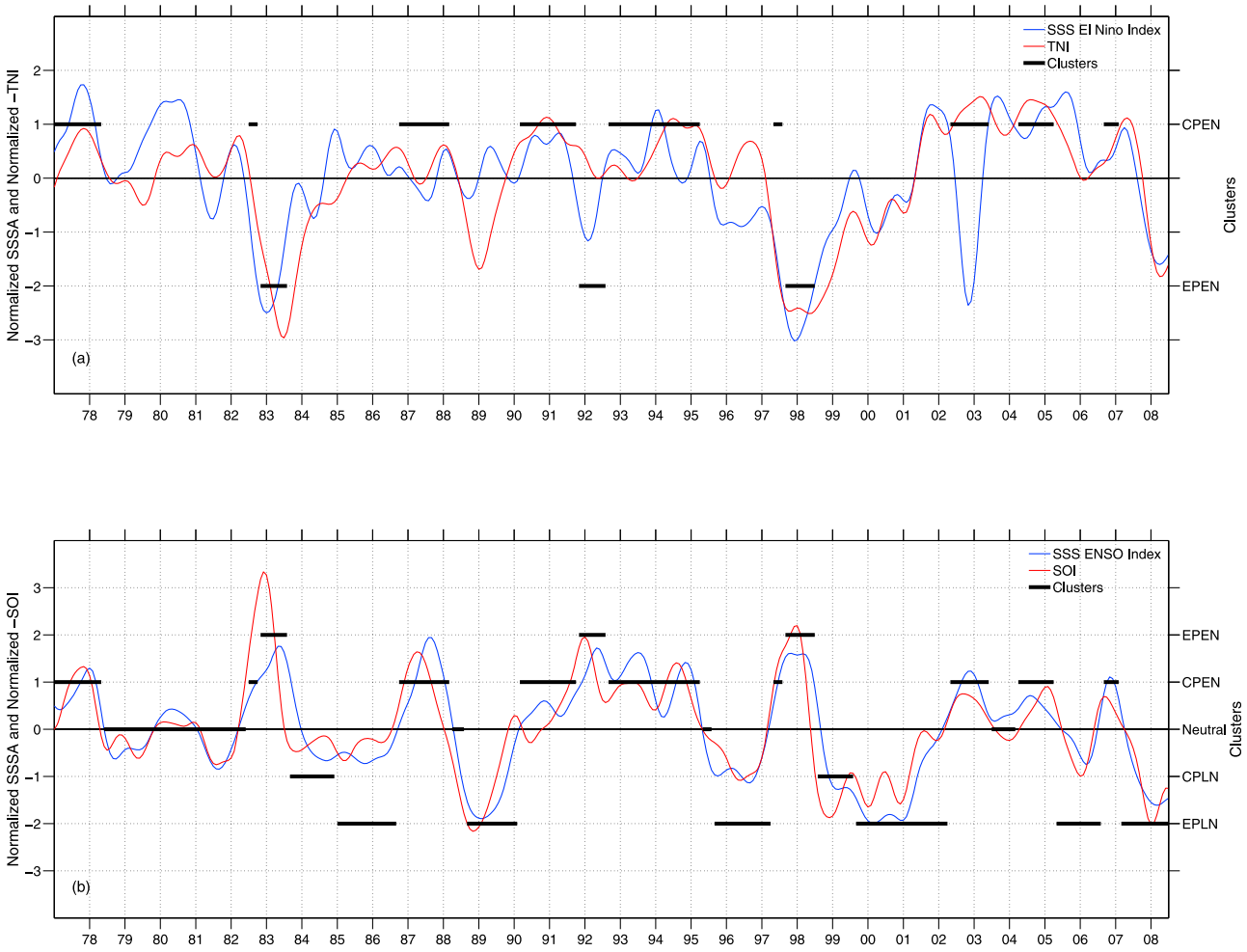

Figure 13. Time series of (a) the SSS El Niño Index and (b) the SSS ENSO Index in blue with the 13 months Hanning filtered SOI and TNI superimposed in red (in Figures 13a and 13b, respectively), and the timing of the SSS clusters in black (see Figure 5). See section 5.4 for the definition of both indices.

SPCZ positions over the entire data length and for each cluster.

[26] The La Niña signal (Figures 11b and 11c) is consistent with the SSSA pattern (Figures 5c and 5d) with negative correlations, respectively, north and south of the SPCZ position. The pattern is reversed during CP and EP El Niño as can be seen in Figures 11a and 11d, respectively. Noteworthy, the SPCZ position does not move as far to the north during CP El Niño as during EP El Niño and, as expected from the derived precipitation changes, the positive SSS anomalies are reduced in magnitude.

[27] The SPCZ position found above is similar to findings by *Vincent* [1994], *Folland et al.* [2002] and *Gouriou and Delcroix* [2002], but only for EP El Niño and La Niña events. Recently, *Vincent et al.* [2009] further characterized the SPCZ position into four different structures using three monthly austral summer precipitation composites over the 1979–2002 period. We reinforce their work by obtaining similar results for the SPCZ position but further stress that this is strongly characterized by the different SSSA structures during EP and CP El Niño and La Niña.

[28] As was done with the precipitation anomalies, the zonal currents anomalies in the SPCZ region were also extracted from the SSS cluster time series with zonal currents leading SSS by 7 months (based on the EOF principal components in SSS and zonal current); the results are shown in Figure 12. In general, the zonal currents anomalies complement the precipitation anomalies (Figure 11) in explaining the SSS signal (Figures 5b–5d) in the SPCZ region with eastward (westward) zonal currents anomalies bringing in fresher (saltier) waters from the southwestern (eastern) tropical Pacific (see the mean SSS structure in Figure 2b).

5.4. Defining ENSO Metrics With SSS

[29] The EOF and AHC procedures indicate that the main difference during EP and CP ENSO is the appearance of contrasted SSS patterns in the equatorial part of the warm pool and along the mean SPCZ position. Because of this we identify three regions in the western half of the tropical Pacific: the first region (A) is delimited between 2°S–2°N and 150°E–170°E, the second (B) between 2°S–2°N and 170°E–170°W and the third (C) between 160°E–160°W and

25°S–10°S. The normalized difference (B-A) between the normalized average SSSA in the first two regions results in an index (Figure 13a), henceforth called the SSS El Niño Index, which is fairly able to distinguish EP El Niño events from CP El Niño events (except in 2003). In fact it has a high negative correlation of R = −0.7 with the TNI (defined as the normalized difference between the normalized SST anomalies averaged in the Niño-1+2 and Niño-4 regions) lagging by 2 months. In addition, because the SSS signature in the SPCZ area is also different during El Niño and La Niña episodes, the normalized difference (C-(A+B)) between the normalized average SSSA in the third (SPCZ) region and the sum of the normalized average SSSA in the first two (equatorial) regions (Figure 13b), hereafter called the SSS ENSO Index, allows us to discriminate between El Niño (positive anomalies) and La Niña (negative anomalies) events, in agreement with the WMO definition in Figure 1. Actually, it has a high correlation of R = −0.88 with the SOI leading by 2 months. Moreover, both indices correspond fairly well with the SSS cluster time series in Figure 5, suggesting that the SSS El Niño Index (SSS ENSO Index) could also be used as an indicator for EP and CP El Niño (and La Niña) events.

6. Conclusion and Discussion

[30] The analyses of resemblances and dissimilarities between ENSO events are both important for improving the understanding of ENSO physics, predicting regional and global climate impacts, and estimating the effects of global warming on ENSO features. Accordingly, both ENSO similarities and differences have been analyzed in the last three decades, probably starting from the milestone papers of *Wyrtki* [1975] and *Rasmusson and Carpenter* [1982]. As stated 35 years ago by K. Wyrtki: "no two El Niño events are quite alike." Since then, numerous results have pointed out the many dissimilarities of ENSO events [e.g., *Wang*, 1995], including the recent detection of a new type of El Niño variously called Dateline, Warm Pool, central Pacific or El Niño Modoki events [*Harrison and Larkin*, 1998; *Larkin and Harrison*, 2005a, 2005b; *Ashok et al.*, 2007; *Kao and Yu*, 2009; *Kug et al.*, 2009]. In line with this, the aim of this paper was to contrast ENSO features in the tropical Pacific, for the first time using SSS observations, as collected during 1977–2008.

[31] Using EOF and AHC analyses on SSS, and comparing with ENSO-related SST features, we showed that the eastern Pacific (EP) El Niño events in SSS appear in 1982–1983, 1991–1992, and 1997–1998, the central Pacific (CP) El Niño events in 1977–1978, 1986–1988, 1990–1991, 1992–1995, 2002–2003, 2004–2005 and 2006–2007, the EP La Niña events in 1985–1986, 1988–1989, 1995–1996, 1999–2001, 2005–2006 and 2007–2008, and the CP La Niña events in 1983–1984 and 1998–1999. It should be noted, however, that clearly differentiating the two EP and CP El Niño and La Niña flavors is a difficult exercise, depending on the method used (see Figure 1), and noting that some years may even be classified as "mixed" events [e.g., *Kug et al.*, 2009, Figure 1]. In general, EP and CP El Niño (La Niña) events result in a SSS freshening (saltening) in the western half of the equatorial Pacific and a SSS increase (decrease) in the SPCZ mean area. The EP and CP El Niño events, however, have distinct quantitative SSS signatures. In the equatorial Pacific (say 2°S–2°N), EP El Niño events are characterized by a maximum SSS freshening (∼−1) near the dateline and a strong (∼30° longitude) eastward displacements of the 34.8 isohaline materializing the eastern edge of the low-salinity warm pool waters. During CP El Niño events, the maximum SSS freshening is shifted westward by about 15° longitude and the eastward displacements of the 34.8 isohaline are only about half the EP El Niño amplitude. *Kug et al.* [2009] found similar differences between Warm Pool and Cold Tongue El Niños (analogous to our CP and EP El Niño) in terms of SST, precipitation, atmospheric vertical motion and surface zonal wind anomalies: the anomalies are shifted to the west during Warm Pool El Niño compared to those associated with the Cold Tongue El Niño. This results in rather homogeneous SSS within 150°E–170°W during EP El Niño events, contrasting with nonhomogeneous SSS between the western (150°E–170°E) and eastern (170°E–170°W) halves of the warm pool during CP El Niño events (with the western half being ∼0.2 fresher). In the far western equatorial Pacific, results are also contrasted: EP El Niño result in a saltening, whereas CP El Niño in a freshening of the surface waters. Besides, in the SPCZ mean area, EP El Niño events are characterized by a well-marked increase (∼+1) in SSS, which is about 2–3 times less during CP El Niño events. As a practical application, we showed that computing SSS differences between the western and eastern parts of equatorial part of the warm pool, as well as between the warm pool and the SPCZ mean areas, which we define as the SSS El Niño and SSS ENSO Indices, could be used as possible indicators of (EP and CP) El Niño and La Niña events, potentially enriching the list of simple ENSO metrics to benchmark climate model skills.

[32] A qualitative analysis of the two main terms of the SSS balance strongly suggests that zonal advection by surface currents and precipitation changes are the main mechanisms responsible for the ENSO signatures in SSS. In the equatorial band, the zonal displacements of the eastern edge of the warm pool (i.e., the 34.8 isohaline) are remarkably consistent with the zonal current anomalies, as demonstrated earlier (see *Picaut et al.* [2001] for a review). Notable differences in zonal currents, however, show up between EP and CP El Niño events. During EP El Niño events, eastward current anomalies appear chiefly from the western to the central eastern equatorial Pacific, consistently with the strong eastward displacements of low-salinity warm pool waters. In contrast, during CP El Niño events, there is a tendency to have a zonal current convergence slightly west of the dateline, consistent with the reduced eastward displacements and, more generally, with the confinement of the warm/fresh pool in the central Pacific basin. The strong eastward displacements of the warm/fresh pool in the equatorial band during EP El Niño events lead to an important northeastward shift of the SPCZ (∼5°–7° latitude for the eastern part) which induces rainfall deficit and related SSS increase at the mean SPCZ position. In contrast, the central Pacific confinement of the warm/fresh pool during CP El Niño events yields to small (∼1°–2° latitude) equatorward shifts of the SPCZ and to moderate SSS increase at the mean SPCZ position.

[33] It has been suggested by *Kao and Yu* [2009] that EP ENSO fits well with the evolution described by the delayed oscillator theory of ENSO, while it is likely that local atmospheric forcing is important to CP ENSO. Accordingly, *Yu et al.* [2010a] showed that their Type 1 SST variability (analogous to our EP El Niño) in the central Pacific results from the zonal advection of thermocline-controlled SST variations from the eastern equatorial Pacific whereas their Type 2 variability (analogous to our CP El Niño) is linked to the northeastern subtropics through surface wind forcing and associated atmosphere-ocean heat fluxes (primarily the latent heat flux) and surface ocean advection. As discussed above, our analysis of SSS changes in the equatorial band during ENSO also suggests that one of the main SSS differences between EP and CP El Niño events result from the different roles of zonal current anomalies, in particular with the zonal currents anomalies favoring the warm pool confinement in the central Pacific during CP El Niño events. The question then remains as to why zonal currents differ so drastically between EP and CP events? One possibility that first comes to mind is the wind stress forcing. As noted by *Kao and Yu* [2009], westerly wind anomalies covered a large part of the tropical Pacific during EP El Niño events, whereas they are limited to its western central part during CP El Niño events. Both instances of westerly anomalies are located west of the maximum related warm SST anomalies, in close agreement with a Gill-type model. Further studies should be carried out to differentiate these coupling processes. Another possibility is that the barrier layer (BL) may be responsible for the different zonal currents anomalies. Model results have shown that its existence in the equatorial part of the warm pool may affect zonal currents [*Vialard et al.*, 2002] and/or ENSO development [*Maes et al.*, 2006]. Previous studies actually suggest a tendency for a thick BL to be associated with the two EP El Niño events in 1991–1992 and 1997–1998, noting that we cannot conclude for the third EP El Niño event in 1982–1983 given the poor data density at that time [*Ando and McPhaden*, 1997; *Maes and Behringer*, 2000; *Vialard et al.*, 2002; *Bosc et al.*, 2009]. Yet, another possibility for the different zonal currents anomalies is the role of equatorial waves. As discussed in previous papers [e.g., *Delcroix and Picaut*, 1998; *Picaut and Delcroix*, 1995], the zonal displacements of the eastern edge of the warm/fresh pool chiefly result from the combined effects of wind-forced and reflected first baroclinic equatorial Kelvin and first meridional mode Rossby waves. The confinement of the warm/fresh pool in the central Pacific basin during CP El Niño events should thus necessarily reflect a specific combination of these waves.

[34] Another interesting question is to what extent changes in the number and amplitude of ENSO events, as well as the respective occurrence of EP and CP events, might contribute to long-term SSS trends, as discussed by *Compo and Sardeshmukh* [2010] and *Lee and McPhaden* [2010] for SST. We showed above from *detrended* SSS time series that CP, as compared to EP El Niño events, are characterized by an increased freshening in the far western equatorial Pacific and a reduced saltening in the SPCZ mean area. Taken as a whole, this can be viewed as a relative freshening of the western half of the tropical Pacific. Hence, assuming that the frequency of CP events will increase with global warming [*Yeh et al.*, 2009], we would thus observe an ENSO-related enhancement of the long-term freshening trends observed in the western half of the tropical Pacific [*Delcroix et al.*, 2007; *Cravatte et al.*, 2009]. Caution will thus be required to properly discriminate natural (ENSO) from anthropogenic (trend) climate changes in long-term SSS records: a generic question in today's climate research.

[35] **Acknowledgments.** This work is a contribution to the GLOSCAL ESA/SMOS proposal supported by CNES. We benefited from numerous observed data sets made freely available, and those which are used in this manuscript include the Hadley Centre Sea Ice and Sea Surface Temperature (http://www.metoffice.gov.uk/hadobs/hadisst/), French Sea Surface Salinity Observation Service (http://www.legos.obs-mip.fr/en/observations/sss/), Global Precipitation Climatology Project (http://www.esrl.noaa.gov/psd/data/gridded/data.gpcp.html), Southern Oscillation Index (http://www.cpc.ncep.noaa.gov/data/indices/soi), El Niño Modoki Index (http://www.jamstec.go.jp/frcgc/research/d1/iod/modoki_home.html.en), Trans-Niño Index (http://www.cgd.ucar.edu/cas/catalog/climind/TNI_N34/index.html), and Ocean Surface Current Analyses-Real time (http://www.oscar.noaa.gov/datadisplay/) data sets. One of us (A.S.) benefits from a Ph.D. grant from the Institut de Recherche pour le Développement (IRD). We also thank the three anonymous reviewers for their constructive comments.

References

Ando, K., and M. J. McPhaden (1997), Variability of surface layer hydrography in the tropical Pacific, *J. Geophys. Res.*, *102*(C10), 23,063–23,078, doi:10.1029/97JC01443.

Ashok, K., S. K. Behera, S. A. Rao, H. Weng, and T. Yamagata (2007), El Niño Modoki and its possible teleconnection, *J. Geophys. Res.*, *112*, C11007, doi:10.1029/2006JC003798.

Ashok, K., S. Iizuka, S. A. Rao, N. H. Saji, and W.-J. Lee (2009a), Processes and boreal summer impacts of the 2004 El Niño Modoki: An AGCM study, *Geophys. Res. Lett.*, *36*, L04703, doi:10.1029/2008GL036313.

Ashok, K., C.-Y. Tam, and W.-J. Lee (2009b), ENSO Modoki impact on the Southern Hemisphere storm track activity during extended austral winter, *Geophys. Res. Lett.*, *36*, L12705, doi:10.1029/2009GL038847.

Barber, C. B., D. P. Dobkin, and H. Huhdanpaa (1996), The quickhull algorithm for convex hulls, *Trans. Math. Software*, *22*(4), 469–483, doi:10.1145/235815.235821.

Bonjean, F., and G. S. E. Lagerloef (2002), Diagnostic model and analysis of the surface currents in the tropical Pacific Ocean, *J. Phys. Oceanogr.*, *32*(10), 2938–2954, doi:10.1175/1520-0485(2002)032<2938:DMAAOT>2.0.CO;2.

Bosc, C., and T. Delcroix (2008), Observed equatorial Rossby waves and ENSO-related warm water volume changes in the equatorial Pacific Ocean, *J. Geophys. Res.*, *113*, C06003, doi:10.1029/2007JC004613.

Bosc, C., T. Delcroix, and C. Maes (2009), Barrier layer variability in the western Pacific warm pool from 2000 to 2007, *J. Geophys. Res.*, *114*, C06023, doi:10.1029/2008JC005187.

Cai, W., and T. Cowan (2009), La Niña Modoki impacts Australia autumn rainfall variability, *Geophys. Res. Lett.*, *36*, L12805, doi:10.1029/2009GL037885.

Chen, G., and C.-Y. Tam (2010), Different impacts of two kinds of Pacific Ocean warming on tropical cyclone frequency over the western North Pacific, *Geophys. Res. Lett.*, *37*, L01803, doi:10.1029/2009GL041708.

Chiodi, A. M., and D. E. Harrison (2010), Characterizing warm-ENSO variability in the equatorial Pacific: An OLR perspective, *J. Clim.*, *23*(9), 2428–2439, doi:10.1175/2009JCLI3030.1.

Compo, G. P., and P. D. Sardeshmukh (2010), Removing ENSO-related variations from the climate record, *J. Clim.*, *23*(8), 1957–1978, doi:10.1175/2009JCLI2735.1.

Cravatte, S., T. Delcroix, D. Zhang, M. McPhaden, and J. Leloup (2009), Observed freshening and warming of the western Pacific warm pool, *Clim. Dyn.*, *33*(4), 565–589, doi:10.1007/s00382-009-0526-7.

Delcroix, T. (1998), Observed surface oceanic and atmospheric variability in the tropical Pacific at seasonal and ENSO timescales: A tentative overview, *J. Geophys. Res.*, *103*(C9), 18,611–18,633, doi:10.1029/98JC00814.

Delcroix, T., and J. Picaut (1998), Zonal displacement of the western equatorial Pacific "fresh pool," *J. Geophys. Res.*, *103*(C1), 1087–1098, doi:10.1029/97JC01912.

Delcroix, T., S. Cravatte, and M. J. McPhaden (2007), Decadal variations and trends in tropical Pacific sea surface salinity since 1970, *J. Geophys. Res.*, *112*, C03012, doi:10.1029/2006JC003801.

Delcroix, T., G. Alory, S. Cravatte, T. Corrège, and M. McPhaden (2011), A gridded sea surface salinity data set for the tropical Pacific with sample applications (1950–2008), *Deep Sea Res., Part I*, *58*(1), 38–48, doi:10.1016/j.dsr.2010.11.002.

Deser, C., and J. M. Wallace (1987), El Niño events and their relation to the Southern Oscillation: 1925–1986, *J. Geophys. Res.*, *92*(C13), 14,189–14,196, doi:10.1029/JC092iC13p14189.

Emery, W. J., and R. E. Thomson (2001), *Data Analysis Methods in Physical Oceanography*, 2nd ed., Elsevier Sci., Amsterdam.

Folland, C. K., J. A. Renwick, M. J. Salinger, and A. B. Mullan (2002), Relative influences of the Interdecadal Pacific Oscillation and ENSO on the South Pacific Convergence Zone, *Geophys. Res. Lett.*, *29*(13), 1643, doi:10.1029/2001GL014201.

Glantz, M. H., R. W. Katz, and N. Nicholls (1991), *Teleconnections Linking Worldwide Climate Anomalies*, Cambridge Univ. Press, Cambridge, U. K.

Global Climate Observing System (2004), Implementation plan for the global observing system for climate in support of the UNFCCC: Executive summary, *Rep. GCOS-92(ES)*, 29 pp., World Meteorol. Organ., Geneva, Switzerland.

Goddard, L., and M. Dilley (2005), El Niño: Catastrophe or opportunity, *J. Clim.*, *18*(5), 651–665, doi:10.1175/JCLI-3277.1.

Gouriou, Y., and T. Delcroix (2002), Seasonal and ENSO variations of sea surface salinity and temperature in the South Pacific Convergence Zone during 1976–2000, *J. Geophys. Res.*, *107*(C12), 3185, doi:10.1029/2001JC000830.

Hanley, D. E., M. A. Bourassa, J. J. O'Brien, S. R. Smith, and E. R. Spade (2003), A quantitative evaluation of ENSO indices, *J. Clim.*, *16*(8), 1249–1258, doi:10.1175/1520-0442(2003)16<1249:AQEOEI>2.0.CO;2.

Harrison, D. E., and N. K. Larkin (1998), El Niño-Southern Oscillation sea surface temperature and wind anomalies, 1946–1993, *Rev. Geophys.*, *36*(3), 353–399, doi:10.1029/98RG00715.

Hendon, H. H., E. Lim, G. Wang, O. Alves, and D. Hudson (2009), Prospects for predicting two flavors of El Niño, *Geophys. Res. Lett.*, *36*, L19713, doi:10.1029/2009GL040100.

Huffman, G. J., R. F. Adler, D. T. Bolvin, and G. Gu (2009), Improving the global precipitation record: GPCP Version 2.1, *Geophys. Res. Lett.*, *36*, L17808, doi:10.1029/2009GL040000.

Janowiak, J. E., A. Gruber, C. R. Kondragunta, R. E. Livezey, and G. J. Huffman (1998), A comparison of the NCEP-NCAR reanalysis precipitation and the GPCP rain gauge-satellite combined dataset with observational error considerations, *J. Clim.*, *11*(11), 2960–2979, doi:10.1175/1520-0442(1998)011<2960:ACOTNN>2.0.CO;2.

Jin, F.-F., J. D. Neelin, and M. Ghil (1994), El Niño on the Devil's Staircase: Annual subharmonic steps to chaos, *Science*, *264*(5155), 70–72, doi:10.1126/science.264.5155.70.

Kalnay, E., et al. (1996), The NCEP/NCAR 40-year reanalysis project, *Bull. Am. Meteorol. Soc.*, *77*(3), 437–471, doi:10.1175/1520-0477(1996)077<0437:TNYRP>2.0.CO;2.

Kao, H.-Y., and J.-Y. Yu (2009), Contrasting eastern-Pacific and central-Pacific types of ENSO, *J. Clim.*, *22*(3), 615–632, doi:10.1175/2008JCLI2309.1.

Kaplan, A., M. A. Cane, Y. Kushnir, A. C. Clement, M. B. Blumenthal, and B. Rajagopalan (1998), Analyses of global sea surface temperature 1856–1991, *J. Geophys. Res.*, *103*(C9), 18,567–18,589, doi:10.1029/97JC01736.

Kim, H.-M., P. J. Webster, and J. A. Curry (2009), Impact of shifting patterns of Pacific Ocean warming on North Atlantic tropical cyclones, *Science*, *325*(5936), 77–80, doi:10.1126/science.1174062.

Kohonen, T. (1989), *Self-Organization and Associative Memory*, 3rd ed., Springer, New York.

Kug, J.-S., F.-F. Jin, and S.-I. An (2009), Two types of El Niño events: Cold tongue El Niño and warm pool El Niño, *J. Clim.*, *22*(6), 1499–1515, doi:10.1175/2008JCLI2624.1.

Lagerloef, G., et al. (2008), The Aquarius/SAC-D mission: Designed to meet the salinity remote-sensing challenge, *Oceanography*, *21*(1), 68–81.

Larkin, N. K., and D. E. Harrison (2002), ENSO warm (El Niño) and cold (La Niña) event life cycles: Ocean surface anomaly patterns, their symmetries, asymmetries, and implications, *J. Clim.*, *15*(10), 1118–1140, doi:10.1175/1520-0442(2002)015<1118:EWENOA>2.0.CO;2.

Larkin, N. K., and D. E. Harrison (2005a), Global seasonal temperature and precipitation anomalies during El Niño autumn and winter, *Geophys. Res. Lett.*, *32*, L16705, doi:10.1029/2005GL022860.

Larkin, N. K., and D. E. Harrison (2005b), On the definition of El Niño and associated seasonal average U.S. weather anomalies, *Geophys. Res. Lett.*, *32*, L13705, doi:10.1029/2005GL022738.

Lee, T., and M. J. McPhaden (2010), Increasing intensity of El Niño in the central-equatorial Pacific, *Geophys. Res. Lett.*, *37*, L14603, doi:10.1029/2010GL044007.

Leloup, J. A., Z. Lachkar, J.-P. Boulanger, and S. Thiria (2007), Detecting decadal changes in ENSO using neural networks, *Clim. Dyn.*, *28*, 147–162, doi:10.1007/s00382-006-0173-1.

Maes, C., and D. Behringer (2000), Using satellite-derived sea level and temperature profiles for determining the salinity variability: A new approach, *J. Geophys. Res.*, *105*(C4), 8537–8547, doi:10.1029/1999JC900279.

Maes, C., K. Ando, T. Delcroix, W. S. Kessler, M. J. McPhaden, and D. Roemmich (2006), Observed correlation of surface salinity, temperature and barrier layer at the eastern edge of the western Pacific warm pool, *Geophys. Res. Lett.*, *33*, L06601, doi:10.1029/2005GL024772.

McPhaden, M. J., and X. Zhang (2009), Asymmetry in zonal phase propagation of ENSO sea surface temperature anomalies, *Geophys. Res. Lett.*, *36*, L13703, doi:10.1029/2009GL038774.

McPhaden, M. J., S. E. Zebiak, and M. H. Glantz (2006), ENSO as an integrating concept in Earth science, *Science*, *314*(5806), 1740–1745, doi:10.1126/science.1132588.

Meyers, G., P. McIntosh, L. Pigot, and M. Pook (2007), The years of El Niño, La Niña, and interactions with the tropical Indian Ocean, *J. Clim.*, *20*(13), 2872–2880, doi:10.1175/JCLI4152.1.

North, G. R., T. L. Bell, R. F. Cahalan, and F. J. Moeng (1982), Sampling errors in the estimation of empirical orthogonal functions, *Mon. Weather Rev.*, *110*(7), 699–706, doi:10.1175/1520-0493(1982)110<0699:SEITEO>2.0.CO;2.

Palmer, T. N., and D. A. Mansfield (1984), Response of two atmospheric general circulation models to sea-surface temperature anomalies in the tropical east and west Pacific, *Nature*, *310*, 483–485, doi:10.1038/310483a0.

Picaut, J., and T. Delcroix (1995), Equatorial wave sequence associated with warm pool displacements during the 1986–1989 El Niño-La Niña, *J. Geophys. Res.*, *100*(C9), 18,393–18,408, doi:10.1029/95JC01358.

Picaut, J., M. Ioualalen, C. Menkes, T. Delcroix, and M. J. McPhaden (1996), Mechanism of the zonal displacements of the Pacific warm pool: Implications for ENSO, *Science*, *274*(5292), 1486–1489, doi:10.1126/science.274.5292.1486.

Picaut, J., M. Ioualalen, T. Delcroix, F. Masia, R. Murtugudde, and J. Vialard (2001), The oceanic zone of convergence on the eastern edge of the Pacific warm pool: A synthesis of results and implications for El Niño-Southern Oscillation and biogeochemical phenomena, *J. Geophys. Res.*, *106*(C2), 2363–2386, doi:10.1029/2000JC900141.

Rasmusson, E. M., and T. H. Carpenter (1982), Variations in tropical sea surface temperature and surface wind fields associated with the Southern Oscillation/El Niño, *Mon. Weather Rev.*, *110*(5), 354–384, doi:10.1175/1520-0493(1982)110<0354:VITSST>2.0.CO;2.

Rayner, N. A., D. E. Parker, E. B. Horton, C. K. Folland, L. V. Alexander, D. P. Rowell, E. C. Kent, and A. Kaplan (2003), Global analyses of sea surface temperature, sea ice, and night marine air temperature since the late nineteenth century, *J. Geophys. Res.*, *108*(D14), 4407, doi:10.1029/2002JD002670.

Smith, T. M., and R. W. Reynolds (2003), Extended reconstruction of global sea surface temperatures based on COADS data (1854–1997), *J. Clim.*, *16*(10), 1495–1510, doi:10.1175/1520-0442-16.10.1495.

Sudre, J., and R. A. Morrow (2008), Global surface currents: A high-resolution product for investigating ocean dynamics, *Ocean Dyn.*, *58*(2), 101–118, doi:10.1007/s10236-008-0134-9.

Trenberth, K. E. (1984), Signal versus noise in the Southern Oscillation, *Mon. Weather Rev.*, *112*(2), 326–332, doi:10.1175/1520-0493(1984)112<0326:SVNITS>2.0.CO;2.

Trenberth, K. E. (1997), The definition of El Niño, *Bull. Am. Meteorol. Soc.*, *78*(12), 2771–2777, doi:10.1175/1520-0477(1997)078<2771:TDOENO>2.0.CO;2.

Trenberth, K. E., and D. P. Stepaniak (2001), Indices of El Niño evolution, *J. Clim.*, *14*(8), 1697–1701, doi:10.1175/1520-0442(2001)014<1697:LIOENO>2.0.CO;2.

Vialard, J., P. Delecluse, and C. Menkes (2002), A modeling study of salinity variability and its effects in the tropical Pacific Ocean during the 1993–1999 period, *J. Geophys. Res.*, *107*(C12), 8005, doi:10.1029/2000JC000758.

Vincent, D. G. (1994), The South Pacific Convergence Zone (SPCZ): A review, *Mon. Weather Rev.*, *122*(9), 1949–1970, doi:10.1175/1520-0493(1994)122<1949:TSPCZA>2.0.CO;2.

Vincent, E. M., M. Lengaigne, C. E. Menkes, N. C. Jourdain, P. Marchesiello, and G. Madec (2009), Interannual variability of the South Pacific Convergence Zone and implications for tropical cyclone genesis, *Clim. Dyn.*, *36*, 1–16, doi:10.1007/s00382-009-0716-3.

Wang, B. (1995), Interdecadal changes in El Niño onset in the last four decades, *J. Clim.*, *8*(2), 267–285, doi:10.1175/1520-0442(1995)008<0267:ICIENO>2.0.CO;2.

Ward, J. H. (1963), Hierarchical grouping to optimize an objective function, *J. Am. Stat. Assoc.*, *58*(301), 236–244, doi:10.2307/2282967.

Weng, H., K. Ashok, S. K. Behera, S. A. Rao, and T. Yamagata (2007), Impacts of recent El Niño Modoki on dry/wet conditions in the Pacific rim during boreal summer, *Clim. Dyn.*, *29*, 113–129, doi:10.1007/s00382-007-0234-0.

Wolter, K., and M. S. Timlin (1998), Measuring the strength of ENSO events: How does 1997/98 rank?, *Weather*, *53*, 315–324.

Wyrtki, K. (1975), El Niño: The dynamic response of the equatorial Pacific Ocean to atmospheric forcing, *J. Phys. Oceanogr.*, *5*(4), 572–584, doi:10.1175/1520-0485(1975)005<0572:ENTDRO>2.0.CO;2.

Yeh, S.-W., J.-S. Kug, B. Dewitte, M.-H. Kwon, B. P. Kirtman, and F.-F. Jin (2009), El Niño in a changing climate, *Nature*, *461*(7263), 511–514, doi:10.1038/nature08316.

Yu, J.-Y., and S. T. Kim (2010), Three evolution patterns of central-Pacific El Niño, *Geophys. Res. Lett.*, *37*, L08706, doi:10.1029/2010GL042810.

Yu, J.-Y., H.-Y. Kao, and T. Lee (2010a), Subtropics-related interannual sea surface temperature variability in the central equatorial Pacific, *J. Clim.*, *23*, 2869–2884, doi:10.1175/2010JCLI3171.1.

Yu, J.-Y., H.-Y. Kao, T. Lee, and S. T. Kim (2010b), Subsurface ocean temperature indices for central-Pacific and eastern-Pacific types of El Niño and La Niña events, *Theor. Appl. Climatol.*, *103*, 337–344, doi:10.1007/s00704-010-0307-6.

S. Cravatte, T. Delcroix, and A. Singh, IRD/LEGOS, UMR 5566, 14 Avenue Edouard Belin, F-31400 Toulouse, France. (awnesh.singh@legos.obs-mip.fr)